Journal of Vacuum Science & Technology A
ACCEPTED MANUSCRIPT
This is the author's peer reviewed, accepted manuscript. However, the online version of record will be different from this version once it has been copyedited and typeset.
PLEASE CITE THIS ARTICLE AS DOI: 10.1116/6.0004265

Impact of vacuum ultraviolet photons on ultrathin negative tone resists for extreme ultraviolet lithography during plasma etching

Shikhar Arvind,[1,2] Roberto Fallica,[2] Philippe Bezard,[2] John Petersen,[2] Stefan De Gendt,[1,2] and Esben W Larsen[2]
[1)] *KU Leuven, Celestijnenlaan 200f, 3001 Leuven, BE*
[2)] *imec, Kapeldreef 75, 3001 Leuven, BE*

(*Electronic mail: shikhar.arvind@imec.be)

(Dated: 20 January 2025)

To achieve further miniaturization of semiconductor devices, extreme ultraviolet (EUV) lithography is employed for patterning at the cutting-edge nodes. This technique necessitates the use of ultrathin resists (less than 50 nm thick) to maintain pattern stability and meet depth of focus requirements. Typical cold plasmas used for dry etching are rich in vacuum ultraviolet photons, which can cause unintended damage to these resists. This can further reduce the etch budget and complicate pattern transfer. Thus, understanding the impact of these plasma photons on ultrathin resists can be crucial for enabling pattern transfer of sub-10 nm features. Here, we investigate the effects of the vacuum ultraviolet photons on three different models of ultrathin negative tone chemically amplified resists (CARs) along with polymethyl methacrylate (PMMA) as a reference positive tone baseline resist. The resists were exposed to vacuum ultraviolet photons using a deuterium lamp, to argon ions using an ion beam etch tool and to argon plasma using an inductively coupled plasma etch tool. Using different characterization techniques, the variations in etch rate, surface roughness, and bulk chemical changes of the resists under different processing conditions were examined. The applicability of the Ohnishi number and ring parameter etch rate models to the resists and processing conditions used was also studied.

I. INTRODUCTION

Extreme ultraviolet (EUV) lithography (EUVL) is now being used for patterning critical layers in state-of-the-art semiconductor devices[1]. But there are still challenges limiting the wide spread adoption of EUV lithography for high volume manufacturing (HVM). Among these is the need for photoresist materials optimized for EUVL[2,3]. EUV photons (λ=13.5 nm, E=92 eV) interact differently than ArF photons (λ=193 nm, E=6.4 eV) with resist polymers. They possess sufficient energy to ionize polymer resist molecules, which typically have an ionization energy between 7 eV to 10 eV[4,5]. This photoionization triggers a cascade of electron generation, accompanied by various molecular relaxation pathways. The precise mechanisms of EUV-resist interactions remain an active area of research, but it is believed to be primarily driven by electrons rather than the EUV photons themselves[5]. Hence, novel EUV resists are needed to accommodate this changing photochemistry and also possess a high absorption cross-section at 13.5 nm for good sensitivity[2]. EUVL also requires the resists to be ultrathin (less than 50 nm) for two main reasons. Firstly, to maintain a low aspect ratio (height to width of a line feature) for avoiding pattern collapse during development[6]. An aspect ratio of 2:1 is typically prescribed for high pattern stability. Secondly, to accommodate the decreasing depth of focus (DOF) of the next generation EUVL tools. The current workhorse EUVL tool (or scanner), uses 13.5 nm light in an optical projection system with a numerical aperture (NA) of 0.33. The next generation EUV scanners have a higher NA of 0.55. They are also referred to as High NA EUV scanners and are currently being prototyped[7,8]. As the NA increases, the DOF of imaging during lithography decreases according to Rayleigh's criteria and recent simulations[6]. This further necessitates the need for ultrathin resists that lie within the reduced DOF for successful imaging in the High NA EUV scanner[9,10].

Currently, one of the main types of EUV resists being used are the positive tone chemically amplified resists (CARs). CARs have been the workhorse resist platform for HVM using 193 nm lithography and hence were the logical starting point for EUV resist exploration. They usually consist of three main components: a polymer backbone, a photoacid generator (PAG), and a base quencher. The polymer backbone is typically a co-polymer with different pendant groups in the repeating unit, each serving a specific function. A common polymer formulation is a co-polymer of hydroxystyrene (HS) and tert-butylmethacrylate (t-BMA), used in environmentally stable chemically amplified positive (ESCAP) resists. The HS group is the "polar group", which is hydrophilic and readily soluble in an aqueous base solvent. In contrast, the t-BMA, which is the "protecting group" or "acid-labile group" is lipophilic, making the co-polymer insoluble in an aqueous base solvent. Upon light exposure during lithography, the PAG decomposes to generate an acid molecule. During the subsequent post exposure bake (PEB), this photogenerated acid diffuses and reacts with the "acid-labile group" of the polymer, switching its polarity from lipophilic to hydrophilic, also referred to as the deprotection reaction. This deprotection reaction in-turn creates more acid molecules which further react with more polymer generating a cascade of acid molecules. This leads to multiple deprotection reactions for a single incident photon, increasing the sensitivity of the resist[11]. This is referred to as the chemical amplification scheme and hence the name of the resist platform. As EUV photochemistry is expected to be primarily electron driven, in the case of EUV exposed CARs, the PAG activation is expected to occur mainly via electrons generated by photoionization of the polymer rather than the direct photodegradation of PAG itself. After the PEB, the wafer is then developed using an appropriate solvent (or developer) to create the final image on the resist. If developer is an aqueous base such as tetramethylammonium hydroxide (TMAH),

Journal of Vacuum Science & Technology A
ACCEPTED MANUSCRIPT
This is the author's peer reviewed, accepted manuscript. However, the online version of record will be different from this version once it has been copyedited and typeset.
PLEASE CITE THIS ARTICLE AS DOI: 10.1116/6.0004265

the exposed regions dissolve thus creating positive image of the mask and this is called positive tone development (PTD). Alternatively, if an organic developer is used, then the exposed regions remain insoluble while the unexposed regions dissolve. This creates in the resist a negative image of the mask and is called negative tone development (NTD). Negative tone imagining can be advantageous in certain scenarios over positive tone imaging[12]. Tarutani et al. showed that for EUV lithography of trench and contact hole patterns, NTD allows for exposure with higher photon number at a reasonably high image contrast compared to PTD[13]. Using organic developer has also been shown to cause less swelling in the resist and better dissolution characteristics compared to conventional TMAH PTD developer[14,15].

Post lithography and development, plasma etching (or dry etching) is used to transfer the pattern from the resist to the layer below. Typically, thin underlayers (UL) are used below the resist to optimize its adhesion[16] and improve lithographic performance[17]. They can either be spin coated like spin-on-glass (SOG)[18] or directly deposited[19]. For the pattern transfer from resist to the UL, cold high-density plasmas are used. These plasmas are rich in vacuum ultraviolet (VUV) photons which have energies between 6 eV to 12 eV[20]. At these energies, the VUV photons can cause unintended damage to resist, which can especially be pronounced for ultrathin resists. Understanding the impact of these VUV photons and their synergism with other plasma species on ultrathin EUV CARs can inform both resist design and etch process development. This, in turn, can help enable the printing of sub-10 nm features for state-of-the-art electronic chips.

Previously, we developed a testing methodology to examine the effect of VUV photons on ultrathin PMMA[21]. In this study, we apply this methodology to three formulations of novel ultrathin NTD CARs along with PMMA as the PTD baseline. While typical etch processes use reactive chemistries like fluorine, chlorine, or oxygen species, we focus on etching in an argon (Ar) plasma. Ar plasma does not have reactive species and thus makes it simpler to decouple the effect of VUV photons and argon ions (Ar^+). Here, we expose the resists to VUV photons using a deuterium lamp, to Ar^+ ions using an ion beam etch (IBE) tool, and to Ar plasma using an inductively coupled plasma (ICP) etch tool. This approach allows us to study the individual interactions of VUV photons and Ar^+ ions with the resists, as well as observe their synergistic behaviors in a plasma. We calculate the average etch rate of all the blanket resist layers under different processing conditions by measuring the thickness change using ellipsometry. The trends in the etch rate are then correlated to both resist chemistry and thickness. Using atomic force microscopy (AFM), we also measure the surface roughness changes induced after processing. Further, using Fourier transform infrared spectroscopy (FTIR), we characterize the bulk chemical changes occurring in the NTD CARs. Finally, we also examine if existing resist etch rate models using Ohnishi number and ring parameter can be extended to the processing conditions and resists used in this study.

II. EXPERIMENTAL SETUP

A. Sample preparation

Three model NTD CARs labelled as **P1**, **P2**, **P3**, along with PMMA as a PTD baseline resist were spin-coated onto 300 mm wafers with a (9 nm SOG)/Si stack. All the resists had a nominal thickness between 38 nm to 40 nm after coating. The composition and loadings of the NTD CARs are shown in Table I. They have the same composition and loading of the PAG (triphenyl sulphonium triflate) and quencher (triphenyl imidazole) . The polymer backbone is a co-polymer with two different pendant groups. The acid labile group is methyl cyclopentyl methacrylate (MCPMA) for all of them. The only variation is in the second pendant group (polar or lactone group). P1 contains norbornene lactone methacrylate (NLM), P2 contains propylene carbonate methacrylate (PCMA) and P3 contains dihydroxy styrene (DHS). The polymer backbone is the majority component of the NTD CARs with a weight fraction of 71.04%, and with a 40:60 weight distribution of the "polar group" and "acid-labile group", respectively. This gives a mole fraction of 28.9%, 32.7% and 39.9% of NLM, PCMA and DHS in P1, P2 and P3, respectively.

Post coating, only the NTD CARs were exposed to an EUV dose of 30 mJ cm^{-2} in imec's NXE3400B scanner using a blanket exposure over a large area. Post exposure these wafers were baked at 90 °C for 60 s followed by development with an organic solution. These exposed and developed NTD CARs are referred to as LITHO samples. The final thickness after exposure and development of the NTD CARs was between 21 nm to 24 nm due to mass loss and shrinking. The final expected chemistry of the deprotected polymer of the NTD CARs is shown in Figure 1.

All the resist coated wafers were then diced into coupons and exposed to three different processing conditions: only VUV photons (PHOTONS), only Ar^+ ions (IONS) and an Ar plasma (PLASMA). The details of the processing conditions are presented in Table II. As described in our previous work[21], we used a 40 s Ar plasma exposure as our baseline process. Then the exposure times for PHOTONS and IONS processing were adjusted to match the thickness of the PLASMA processed PMMA. To further compare the behavior of the NTD CARs with respect to PMMA, they were all processed under the same IONS, PHOTONS and PLASMA conditions as obtained for PMMA.

B. Inductively coupled plasma etch tool

An industrial ICP source (Lam Research *Kiyo*®) for 300 mm wafers operating at 13.56 MHz was used for all the plasma exposures in the study. An Ar plasma with source power of 1000 W, Ar gas pressure of 10 mTorr and no bias was used. The majority of the VUV photons in an Ar plasma are between λ = 100 nm to 110 nm[22]. This is due to transitions of the first excited resonance states of Ar, i.e., $1s_2$ and $1s_4$ (in Paschen notation) to the ground state, corresponding to λ = 104.8 nm and λ = 106.7 nm respectively[23].

ACCEPTED MANUSCRIPT
Journal of Vacuum Science & Technology A
This is the author's peer reviewed, accepted manuscript. However, the online version of record will be different from this version once it has been copyedited and typeset.
PLEASE CITE THIS ARTICLE AS DOI: 10.1116/6.0004265

Resist	Co-Polymer (40/60 wt%)		PAG	Quencher
P1	NLM	MCPMA	Triphenyl sulphonium triflate	Triphenyl imidazole
P2	PCMA	MCPMA		
P3	DHS	MCPMA		
Loadings (wt%)	71.04		23.04	5.92

TABLE I. The composition of the three model NTD CARs – P1, P2 and P3. The only variation between them is in the polar or lactone group. NLM - norbornene lactone methacrylate, PCMA - propylene carbonate methacrylate, DHS – dihydroxy styrene, MCPMA - methyl cyclopentyl methacrylate. The loadings of each component of the CAR are given by their respective weight fraction (wt%). The co-polymer fractions are also given by the wt%.

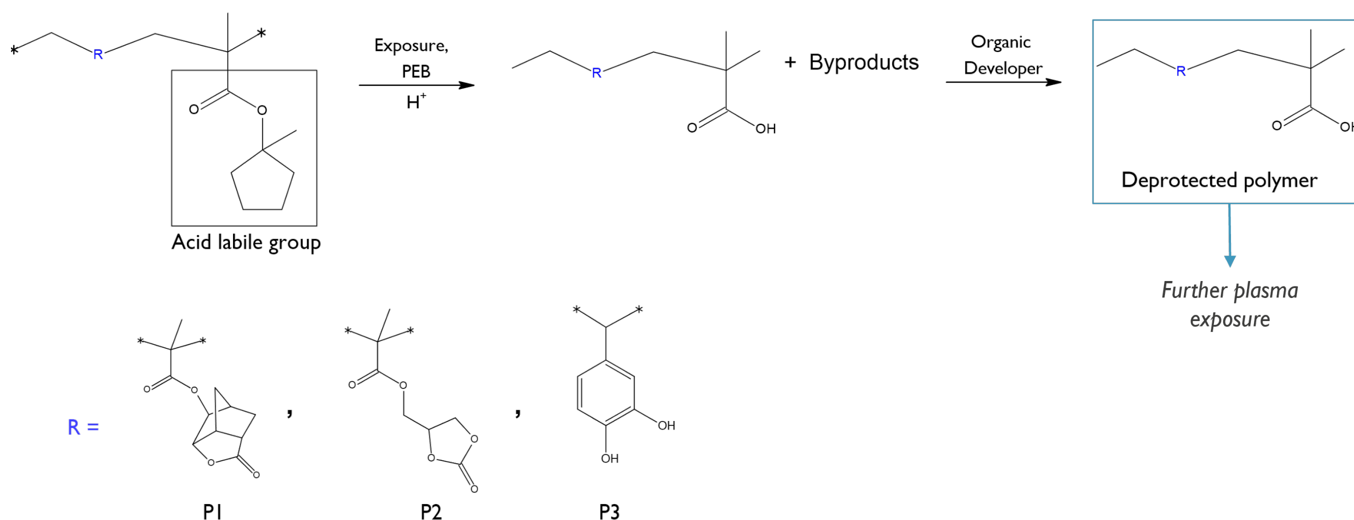

FIG. 1. Simplified chemistry change of NTD CARs during lithography and development. PEB – post exposure bake. The solubility of the resist switches from lipophilic to hydrophilic after lithography and PEB. The final deprotected polymer undergoes further plasma exposure during etching.

C. VUV Photon Lamp

A commercial deuterium lamp (Hamamatsu L12542) was used as the source of VUV photons. The lamp was allowed to stabilize for 1 h before exposures and the stabilized flux was measured using a 1 cm^2 Si photodiode (Opto Diode Corp AXUV100G). The VUV spectrum of the lamp has a peak around 160 nm as per the data provided by the supplier. For more details on flux calculations please refer to the details published in our previous study[21].

D. Ion beam etch tool

An industrial IBE tool (IBE-NX , *ANELVA*™ platform by Canon) using remote Ar plasma was used to expose Ar^+ ions

Journal of Vacuum Science & Technology A ACCEPTED MANUSCRIPT
This is the author's peer reviewed, accepted manuscript. However, the online version of record will be different from this version once it has been copyedited and typeset.
PLEASE CITE THIS ARTICLE AS DOI: 10.1116/6.0004265

Processing condition	Sample size	Processing conditions	Processing time(s)
PLASMA	3 cm x 3 cm Attached to a Si carrier wafer (300 mm).	ICP etch tool, Ar plasma, No bias, Source power = 1000 W, Pressure = 10 mTorr.	40
PHOTONS	2 cm x 2 cm	VUV Lamp, Pressure = 1×10^{-5} mbar, Working Distance≈30 cm.	2200
IONS	3 cm x 3 cm Attached to a Si carrier wafer (300 mm).	IBE tool, Ion energy = 50 eV (lowest possible setting) Pressure = 5×10^{-5} Pa	35

TABLE II. Details of the different processing conditions used in this study.

on the samples. The lowest possible ion energy setting, i.e., 50 eV, was used. An ion current of 400 mA was measured for a full 300 mm wafer exposure.

E. Sample characterization

The samples in this study were characterized using spectroscopic ellipsometry, atomic force microscopy (AFM) and infrared spectroscopy (FTIR). Ellipsometry was used to measure the thickness and refractive index of the samples. AFM was used for surface roughness measurement. Attenuated total reflection (ATR) Fourier transform infrared spectroscopy (FTIR) was used to measure the infrared (IR) spectra of the samples for chemical characterization. Refer to the supplementary material for more details on these techniques. The thickness, refractive index and surface roughness values were measured on various locations on multiple samples for each processing and resist combination. The nominal value reported is the mean and the error bar is the standard deviation of these measured values.

III. RESULTS AND DISCUSSION

IV. ETCH RATE

The average consumption rate, or etch rate (ER), of all the resists under different processing conditions was calculated and plotted in Figure 2 by measuring the thickness before and after processing.

From the Figure 2, the ER of the resists follow a similar trend under the three processing conditions i.e., ER (PMMA) > ER (P2) > ER (P1) > ER (P3). The higher ER of PMMA compared to NTD CARs is mainly due to its thicker film and simpler chemistry. Since PMMA was used as a baseline PTD resist, it has a higher starting thickness (38 nm) compared to NTD CARs (21 nm to 24 nm). Vourdas et al previously reported a decreasing ER of PMMA with decreasing thickness in O_2 plasma[24]. They also observed a strong correlation between the decreasing ER and increasing glass transition temperature (T_g) for thinner films and this was mainly attributed to polymer-substrate interaction (or substrate effect). If the substrate-polymer interaction is attractive, as in the case of PMMA with glassy substrates like native oxide or spin-on-glass materials, the substrate effect slows the polymer dynamics, typically leading to an increase the glass transition temperature (T_g) of the polymer leading to slower kinetics and reduced etch rate[24,25]. To further validate this behavior, we spin-coated an experimental 22.5 nm thick PMMA and exposed it to the same processing conditions. We observe a significant reduction in the ER of the thin PMMA under PHOTONS and PLASMA processing compared to its thicker counterpart, whereas under IONS processing only a minor change was observed. An explanation for this is by considering the region of interaction of VUV photons compared to Ar^+ ions. VUV photons penetrate the entire polymer film at the ultrathin thicknesses used in this study[26]. This makes the photodegradation process highly sensitive to the substrate effect which varies with the thickness of the polymer and is strongest as the bottom of the polymer film. In contrast, the Ar^+ ions primarily interact with the polymer's surface/near surface region[21,27] which is the furthest from the substrate and are thus less sensitive to the substrate effect. This can then result in a similar ER independent of the starting thickness.

We see that the thin PMMA still has higher ER compared to P1 and P3 in all processing conditions. This can be attributed to the simple aliphatic chemistry of PMMA. It does not have carbon rich alicyclic or stable aromatic side groups like that in P1 (NLM) and P3 (DHS). The presence of these groups typically leads to lower ion[28,29]and photon degradation[27].

When comparing the ER between the NTD CARs, the main source of difference is the chemistry as their thicknesses are quite similar. P3 with the aromatic DHS group shows the lowest ER in all processing conditions. This can be attributed to the excellent radiation stability of aromatic groups coupled with the higher concentration of DHS in P3. Specifically, the mole fraction of DHS in P3 (39.9%) is higher than MCPMA in P1 (28.9%) and PCMA in P2 (32.7%). Aromatic groups can absorb and dissipate external radiation energy with minimal polymer damage due to resonance stabilization[29,30]. In the case of P1 vs P2 , despite P2 having a higher mole fraction of PCMA, the higher effective carbon content of the bulkier NLM side group in P1 imparts it higher etch resistance[31,32].

The differences in the ER between the NTD CARs in different processing conditions can also impact patterned structures. Since the ions are usually incident close to perpendicular in typical etch processes, they mainly affect the vertical etch rate while VUV photons are isotropic and can penetrate

ACCEPTED MANUSCRIPT
Journal of Vacuum Science & Technology A
This is the author's peer reviewed, accepted manuscript. However, the online version of record will be different from this version once it has been copyedited and typeset.
PLEASE CITE THIS ARTICLE AS DOI: 10.1116/6.0004265

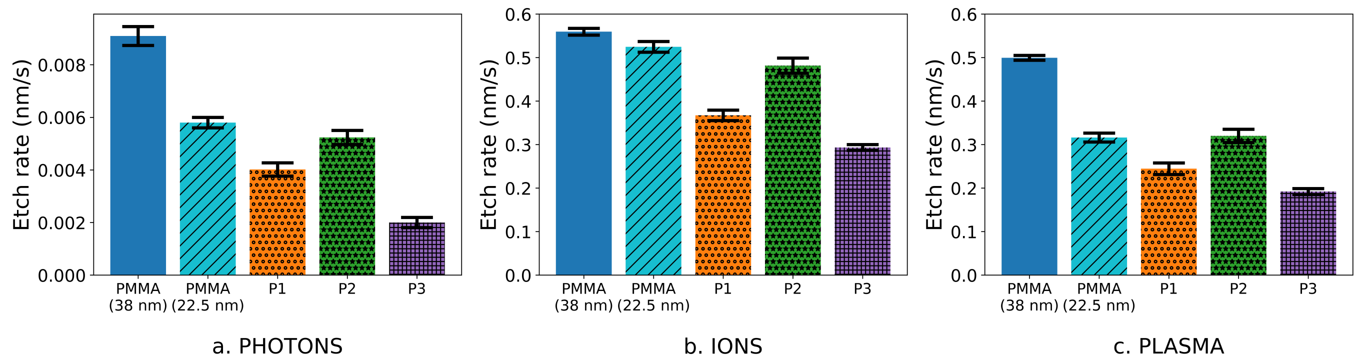

FIG. 2. Average etch rates of the resists under different processing conditions. A thin PMMA (22.5 nm) thick was also coated to evaluate the impact of the starting thickness on the etch rate.

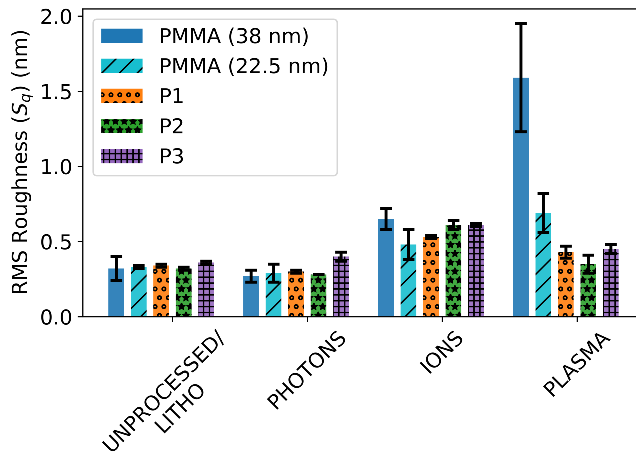

FIG. 3. Surface roughness of different samples for all processing conditions. UNPROCESSED/LITHO corresponds to the starting roughness values of the resists before processing.

the film from different directions, affecting both vertical and lateral etch rates. The variations in ER under ion and photon exposure can lead to different etch anisotropy and pattern profile between the resists for the same etch process.

V. SURFACE ROUGHNESS

To understand the surface profile changes after processing, root mean square surface roughness (S_q) was measured before and after processing for all the resists and is plotted in Figure 3. The starting roughness values for all the resists was between 0.3 nm to 0.35 nm indicating a smooth surface. For the methacrylate-based polymers, i.e., PMMA, P1 and P2, VUV photon exposure reduces S_q slightly while for the phenolic polymer P3, S_q increases. Methacrylate based polymers undergo preferential scissioning during VUV photon exposure[33].VUV photons efficiently attack the C=O bonds in side groups of these polymers, leading to chain scission[33]. This can in turn allow for polymer to reflow, thus decreasing the roughness. Similar smoothening effect by VUV photons on 193 nm resists was observed by Pargon et al[34] and Weilenboeck et al[35]. In the case of P3, the presence of phenolic DHS leads to preferential crosslinking over scissioning[33]. Unlike scissioning, crosslinking does not allow for easier polymer reflow. It can lead to polymer aggregation, thus increasing the S_q[36], as observed for P3. A possible implication of this result for patterned structures with these resists is that plasma or photon smoothening of P3 may be more limited compared to P1 and P2. The surface roughness of all the resists after IONS processing was similar (≈0.6 nm) . This suggests that while the ion ER of the resists varies with their chemistry, the surface profile variations of the ion-modified layer between the resists is minimal. Interestingly, for the PLASMA processed resists, the NTD CARs and the thin PMMA show a lower S_q compared to thick PMMA sample. The exact reasons for this are not fully clear but a closer look at the thick PMMA AFM scan shows reticulation with wrinkle-like structures as shown in Figure 4. Pal et al studied the real time evolution of reticulation on thick 193 nm and 248 nm resists under plasma exposure[37]. They observed that reticulation is induced due to the compressive stresses between ion-modified layer and the bulk beneath it when the resist is heated beyond its T_g. Due to the substrate effect, the T_g of the thick PMMA is expected to be lower than the other thinner resists. A possible explanation for the high S_q of thick PMMA under plasma processing is that due to localized plasma heating and its low T_g, the resist experiences temperatures beyond its T_g . At these temperatures, the stresses between the ion-modified carbonized layer at the top and photon-modified bulk below are high, leading to the reticulation of the thick PMMA surface and a high S_q. Nest et al[38] and Jinnai et al[39] have also reported high surface roughness formation on 193 nm resists in a plasma to be a synergistic effect of ions, VUV photons and temperature. The results from this study are consistent with their findings and additionally highlights the importance of substrate-resist interaction for ultrathin resists. The change in the polymer dynamics and further the T_g due to the low thickness can become a major factor in determining the final structural properties of the plasma-processed resists. In addition to this, we also expect other factors, such as the simul-

ACCEPTED MANUSCRIPT
Journal of Vacuum Science & Technology A
This is the author's peer reviewed, accepted manuscript. However, the online version of record will be different from this version once it has been copyedited and typeset.
PLEASE CITE THIS ARTICLE AS DOI: 10.1116/6.0004265

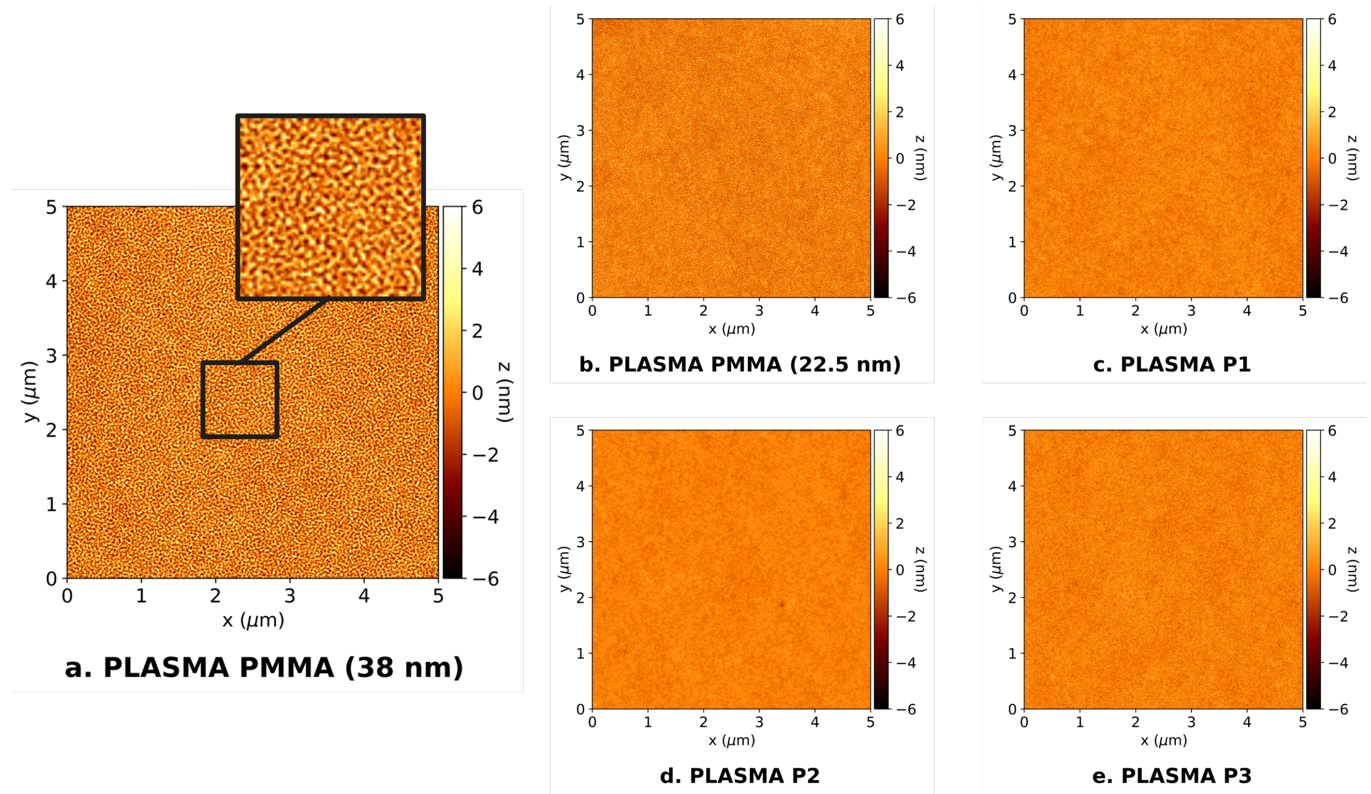

FIG. 4. Surface scans from AFM of the PLASMA processed a. PMMA (38 nm) , b. PMMA (22.5 nm), c. P1, d. P2 and e. P3. The thick PMMA shows reticulation with wrinkle like features on the surface which has been zoomed in for better visualization.

taneous interaction of photogenerated bulk volatile products with the top ion-modified layer, the size and nature of the outgassed products, and the final thickness and chemistry of the processed resist, to also impact the S_q. Decoupling these factors is non-trivial, and additional research is needed to shed more light on the mechanism of surface roughness evolution of ultrathin resists in plasma.

VI. REFRACTIVE INDEX

Figure 5 illustrates the refractive index $n(\lambda)$ of the NTD CARs under different processing conditions as obtained by ellipsometry. The change in the refractive index of the processed resists relative to the unprocessed (LITHO) sample, $\Delta n(\lambda)$ is also plotted in Figure 6. The $n(\lambda)$ increases after processing for all 3 CARs and the trend is as observed previously for PMMA[21]. The IONS processed samples exhibit the highest $\Delta n(\lambda)$. This increase is attributed to the presence of a strongly carbonized ion-modified layer at the surface. The presence of this layer was further validated by observing the sputter times of these films during depth profiling for X-ray photoelectron spectroscopy (XPS). An Ar gas cluster ion beam (GCIB) with energy of 2.5 eV/atom was used as the sputter beam for depth profiling. The sputter time of a film depends both on its thickness and chemistry. Ar GCIB is efficient at sputtering organic materials, but inorganic materials like amorphous carbon are quite sputter resistant to it[40], and hence take longer time to be cleared. For each NTD CAR, the IONS processed film has the longest sputter time despite being the thinnest (Refer supplementary material for the table with sputter times). This further supports the presence of a carbonized layer at the top due to ions and is also in line with our observation on PMMA[21]. Based on previous experimental[21,41,42] and simulation[43] studies, the thickness of this carbonized layer is expected to be around a few nanometers (<5 nm). Given the varying chemistry of the NTD CARs, some variation in deoxygenation and dehydrogenation leading to carbonization is also expected. This variation can result in the NTD CARs having carbonized layers with differing thicknesses and refractive indices. The PHOTONS processed samples exhibit a moderate increase in $n(\lambda)$, typically due degradation of oxygen rich side chains, further leading to an increase in the volumetric density[44–46] and molar refractivity[47]. The PLASMA processed resists have $n(\lambda)$ in between the IONS and PHOTONS processed resists due to both photons and ions modification. The difference in $n(\lambda)$the IONS and PLASMA processed resists can be attributed to difference in the degree of carbonization at the surface. The Ar^+ ion energy in a plasma with no bias is around 15 eV to 20 eV[48] (PLASMA) compared to 50 eV in the IBE (IONS). The higher ion energy coupled with the expectedly higher dose can lead to a thicker[49] and denser[50–52] carbonized layer in the IONS processed resists compared to their PLASMA processed counterparts which can in turn lead to higher $n(\lambda)$.

ACCEPTED MANUSCRIPT
Journal of Vacuum Science & Technology A
This is the author's peer reviewed, accepted manuscript. However, the online version of record will be different from this version once it has been copyedited and typeset.
PLEASE CITE THIS ARTICLE AS DOI: 10.1116/6.0004265

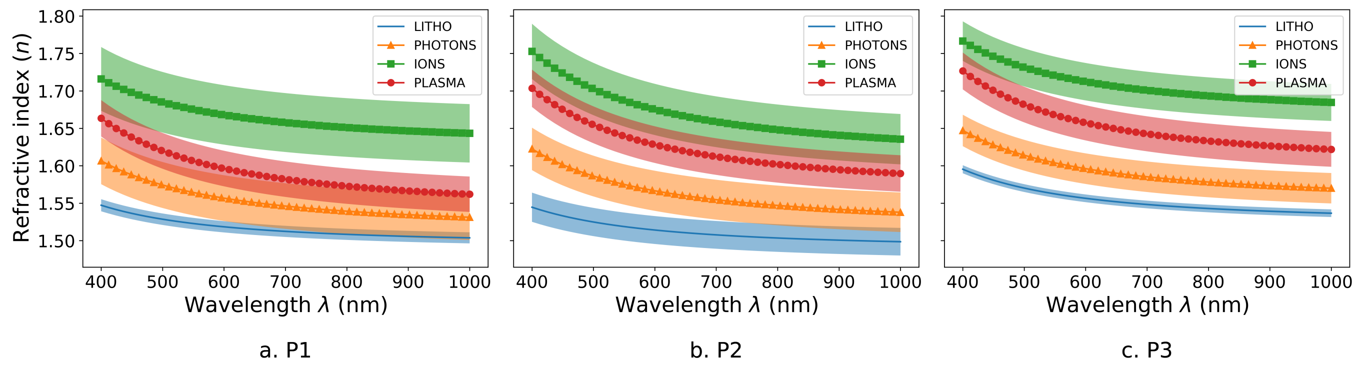

FIG. 5. Refractive index $n(\lambda)$ of the three NTD CARs a. P1 , b. P2 and c. P3 after different processing conditions. The plotted nominal value represents the mean $n(\lambda)$ and the shaded area represents the standard deviation.

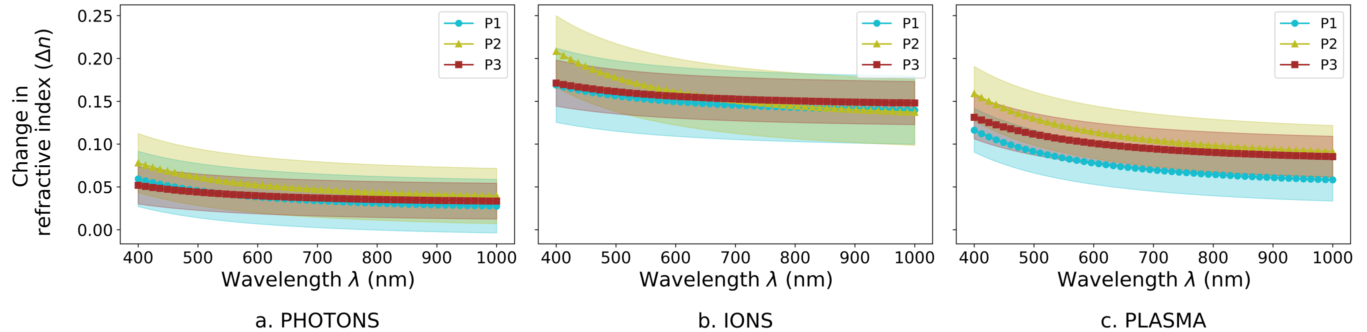

FIG. 6. Change in refractive index $\Delta n(\lambda)$ of the three NTD CARs relative to the unprocessed (LITHO) after a. PHOTONS, b. IONS and c. PLASMA processing.

VII. IR SPECTRA

To further understand the changes in bulk chemistry of the NTD CARs, the IR spectra of the samples were measured. Here, we focus on the C=O region of the IR spectrum. The C=O region exhibits high intensity due to its large dipole moment[53] and shows distinct peaks for the side chain groups. Other interesting IR regions, such as the C−H stretch, C-C stretch, and C=C stretch, did not exhibit sufficient intensity for clear analysis.

Figure 7 shows the C=O IR spectra for the three NTD CARs under different processing conditions. The spectra were baseline corrected. We observe two distinct peaks in the C=O region for P1 and P2 corresponding to the lactone and ester groups in the polymer. The higher wavenumber peak corresponds to lactonic C=O whereas the lower wavenumber peak is for the esteric C=O. In the case of P3, we observe only ester C=O peak from the deprotected side group as expected.

Previously, we observed that for PMMA, IONS primarily modify the top layer of the polymer, leaving a pristine polymer layer beneath. A similar behavior is observed for the NTD CARs. Specifically, in P1 and P2, the IONS sample shows a clear two-peak spectrum, indicating the presence of a buried, pristine-like layer.

We also observe that the lactone side groups in P1 and P2 are readily degraded by VUV photons. There is still a minor C=O peak at the lower wavenumber from residual esteric C=O and other byproducts containing C=O. The high susceptibility of the lactonic C=O has also been observed on thicker 193 nm resists[39,54,55]. Jinnai et al reported that the lactonic C=O is more chemically reactive compared to esteric C=O , and proposed that this is due to the high polarization of lactonic C=O[54]. Similar behavior of lactonic C=O compared to the esteric C=O was also reported by Uesugi et al[56].

In addition to measuring IR spectra post processing, it would be interesting to measure the real-time evolution of IR spectra, as this would enable us to correlate chemical changes with varying etch rates. Although our current testing setup does not allow for this, it could be a focus for future research.

VIII. ETCH RATE MODELS

Etch rate models are used to correlate the ER of resists to their chemistry. These models help to guide the development of new resists by predicting their etch behavior. Two popular models that have been used previously are the Ohnishi number ($O.N.$) and the ring parameter (r) models. The details of these models are presented in Table III. $O.N.$ was introduced by Gokan et al[31] and was mainly successful in predicting the ER of resists under ion beam etch with high energy ions (300 eV to 500 eV). Ring parameter (r) model was later

ACCEPTED MANUSCRIPT
Journal of Vacuum Science & Technology A
This is the author's peer reviewed, accepted manuscript. However, the online version of record will be different from this version once it has been copyedited and typeset.
PLEASE CITE THIS ARTICLE AS DOI: 10.1116/6.0004265

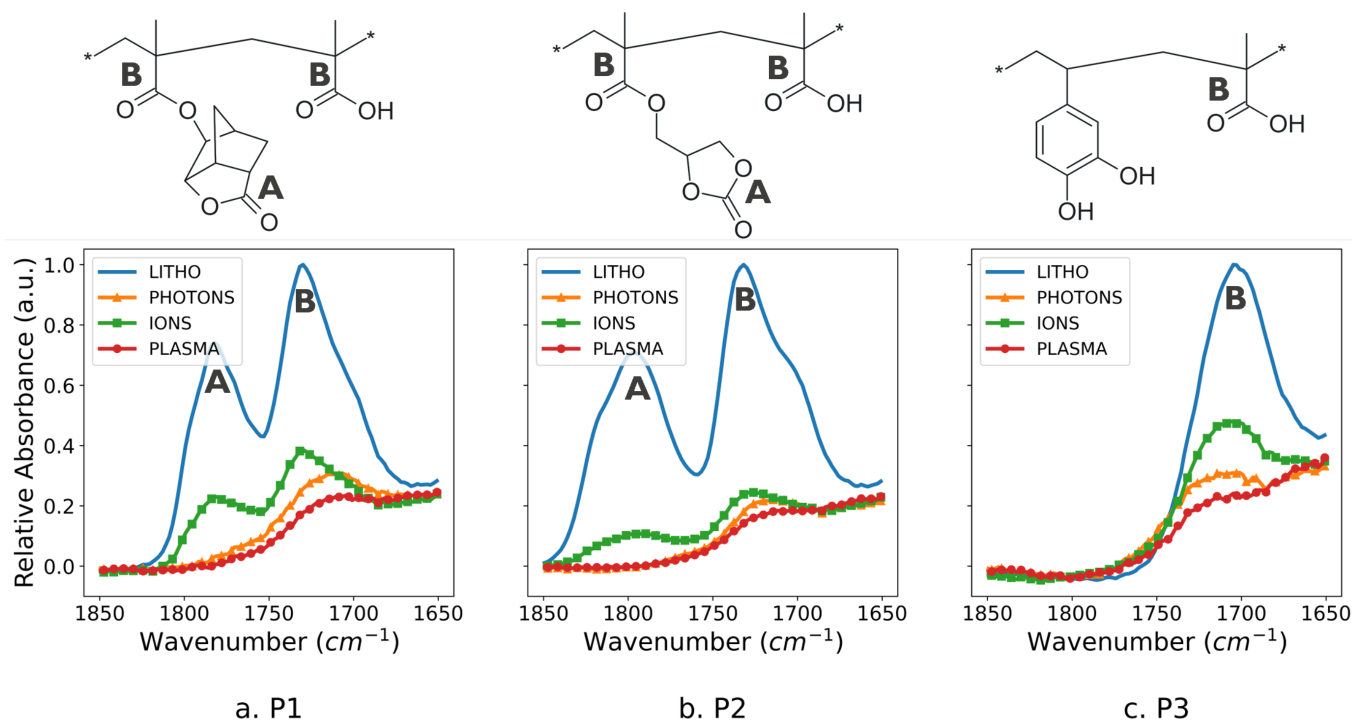

FIG. 7. IR spectra of the C=O region of the NTD CARs a. P1, b. P2 and c. P3. The top chemical structure corresponds the deprotected polymer of each NTD CAR. A and B peaks in P1 and P2 correspond to the lactonic and ester C=O vibrations, respectively (C=O contribution from SOG is negligible, data not shown).

Model	Details
Ohnishi Number ($O.N.$)	$ER \propto O.N. = \frac{N}{N_c - N_o}$ ER - etch rate , N - total number of atoms in the monomer or repeating unit, N_c -Number of carbon atoms in the repeating unit, N_o - Number of oxygen atoms in the repeating unit
Ring parameter (r)	$ER\ (vs\ SPR511) = Ar^3 + Br^2 + Cr + D$ $r = \frac{Mass\ of\ carbon\ atoms\ in\ the\ ring}{Total\ mass\ of\ resist}$ $ER\ (vs\ SPR511)$ – Etch rate normalized to etch rate of resist Shipley SPR511 A, B, C, D – Polynomial fit constants

TABLE III. Details of the etch rate models that are evaluated in this study.

introduced by Kunz et al[57] to accommodate the improved etch resistance of the 193 nm resists with ring structures in a Cl_2 plasma. In addition to these two models, various other models have been developed to predict the etch rate of resists with different chemistry in different plasmas[58–63].

Although the $O.N.$ and r models were originally designed for different processing conditions, we want to test if they can be extended to EUV resists under the specific conditions used in this study. For this, the ER of these resists are plotted against their $O.N.$ (as shown in Figure 8) and r (as shown in Figure 9). For the calculation of $O.N.$ and r of the NTD CARs, the deprotected polymer was used as shown in Figure 1.

Resists with higher $O.N.$ and lower r are expected to show higher ER. We did not perform a statistical fit due to the insufficient number of data points for a reliable analysis. For $O.N.$ model, we focus on IONS processing as it is the closest to the conditions used when developing the model. Here, P2 has a higher $O.N.$ than PMMA but shows a lower ER. This is possibly due to $O.N.$ not accounting for the added stability of the ring structure of PCMA in P2. Similarly, for r model we mainly focus on the PLASMA processing as it is the closest to conditions used when developing the model. For the PLASMA processed films, there is a minor discrepancy when comparing P2 to thin PMMA under PLASMA processing. In this case P2 has a higher r than PMMA but also shows a higher ER. This could be due to the r model not accounting for the exact nature of the bonds within the ring structure. There is also the expected discrepancy in both models between the thick and thin PMMA as both have same $O.N.$ and r but different etch rates.

The $O.N.$ and r model predict the resist trends well for the different processing conditions and resists used in this study.

Journal of Vacuum Science & Technology A
ACCEPTED MANUSCRIPT
This is the author's peer reviewed, accepted manuscript. However, the online version of record will be different from this version once it has been copyedited and typeset.
PLEASE CITE THIS ARTICLE AS DOI: 10.1116/6.0004265

The models could be further improved if they could also account for the initial thickness of the resist, especially at the ultrathin regimes. Since these models were designed for mainly organic resists, their applicability to novel hybrid EUV resists like metal oxide resists is yet to be determined.

IX. CONCLUSION

In this study we investigated the impact of VUV photons on three ultrathin model NTD CARs along with PMMA as a reference baseline. We observed that thinner PMMA exhibited lower etch rate compared to a thicker film due to a more pronounced effect of the substrate, leading to slower etch kinetics. For the NTD CARs, polymers with aromatic groups and high effective carbon content also exhibited lower etch rates. VUV photons significantly degraded the carbonyl groups throughout the bulk of these resists and caused smoothening or roughening of the surface depending on the chemistry of the resist. Ar^+ predominantly affected the top of the film, creating a carbonized ion-modified layer. The plasma-exposed resists exhibited a more complex pattern of surface roughness variation with factors like the stresses between the ion-modified layer and photo-modified bulk, substrate-effect and the plasma heating affecting it. In this study we investigated the impact of VUV photons on three ultrathin model NTD CARs along with PMMA as a reference baseline. We observed that thinner PMMA exhibited lower etch rate compared to a thicker film due to a more pronounced effect of the substrate, leading to slower etch kinetics. For the NTD CARs, polymers with aromatic groups and high effective carbon content also exhibited lower etch rates. VUV photons significantly degraded the carbonyl groups throughout the bulk of these resists and caused smoothening or roughening of the surface depending on the chemistry of the resist. Ar^+ ions predominantly affected the top of the film, creating a carbonized ion-modified layer. The plasma-exposed resists exhibited a more complex pattern of surface roughness variation with factors like the stresses between the ion-modified layer and photo-modified bulk, substrate-effect and the plasma heating affecting it. Due to limitations of the current testing setup, the individual effects of plasma heating, electrons and Ar metastable neutrals could not be investigated, but these factors can also contribute to the degradation of the resists in a plasma[38,64]. Ohnishi number and ring parameter etch rate models were also tested for resist behavior in the different processing conditions used, and they seem to work well. The applicability of current etch rate models for novel non-CAR resists for EUV lithography is yet to be determined.

SUPPLEMENTARY MATERIAL

An additional supplementary document is included with more details on the metrology techniques used and sputter times of different films during XPS depth profiling.

ACKNOWLEDGEMENT

The authors would like to thank FUJIFILM for providing the model resist samples used in this study. The authors would like to thank Materials Characterization and Analysis (MCA) group at imec for their help with AFM and XPS analysis. The authors would also like to thank Shreya Kundu and Laura Galleni at imec for their help with IBE tool and FTIR analysis, respectively. The authors acknowledge funding from the imec Industrial Affiliation Program (IIAP). Shikhar Arvind acknowledges funding from KU Leuven for their doctoral studies.

AUTHOR DECLARATION

A. CONFLICT OF INTEREST

The authors declare no conflict of interest.

B. AUTHOR CONTRIBUTIONS

Shikhar Arvind: Conceptualization (equal); Investigation (lead); writing – original draft (lead); formal analysis (lead); writing – review and editing (equal) **Roberto Fallica:** Conceptualization (equal); Investigation (equal); formal analysis (supporting); Supervision (equal); writing – review and editing (equal) **Philippe Bezard:** Conceptualization (equal); Investigation (equal); formal analysis (supporting); Supervision (equal); writing – review and editing (equal) **John Petersen:** Conceptualization (equal); Investigation (equal); formal analysis (supporting); Supervision (equal); writing – review and editing (equal) **Stefan De Gendt:** Conceptualization (equal); Investigation (equal); formal analysis (supporting); Supervision (equal); writing – review and editing (equal) **Esben W Larsen:** Conceptualization (equal); Investigation (equal); formal analysis (supporting); Supervision (equal); writing – review and editing (equal)

DATA AVAILABILITY

The data that support the findings of this study are available from the corresponding author upon reasonable request.

X. REFERENCES

[1] P. Klomp, R. Es, S. Young, and C. Smeets, "0.33 NA EUV systems for high-volume manufacturing," in *Optical and EUV Nanolithography XXXVII*, Vol. PC12953 (SPIE, 2024) p. PC129530O.
[2] T. Manouras and P. Argitis, "High Sensitivity Resists for EUV Lithography: A Review of Material Design Strategies and Performance Results," Nanomaterials **10**, 1593 (2020).
[3] T. Kozawa, "Design strategy of extreme ultraviolet resists," Japanese Journal of Applied Physics **63**, 050101 (2024).

ACCEPTED MANUSCRIPT
Journal of Vacuum Science & Technology A
This is the author's peer reviewed, accepted manuscript. However, the online version of record will be different from this version once it has been copyedited and typeset.
PLEASE CITE THIS ARTICLE AS DOI: 10.1116/6.0004265

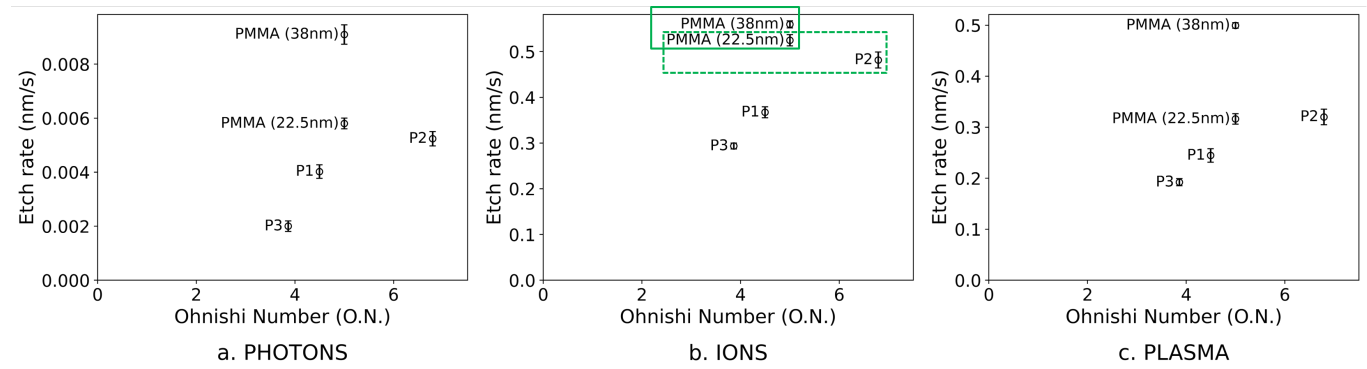

FIG. 8. Average etch rates of different resists compared with their Ohnishi number ($O.N.$) under a. PHOTONS, b. IONS and c. PLASMA processing conditions. Solid box – thickness discrepancy of PMMA. Dashed box – discrepancy between P2 and thin PMMA

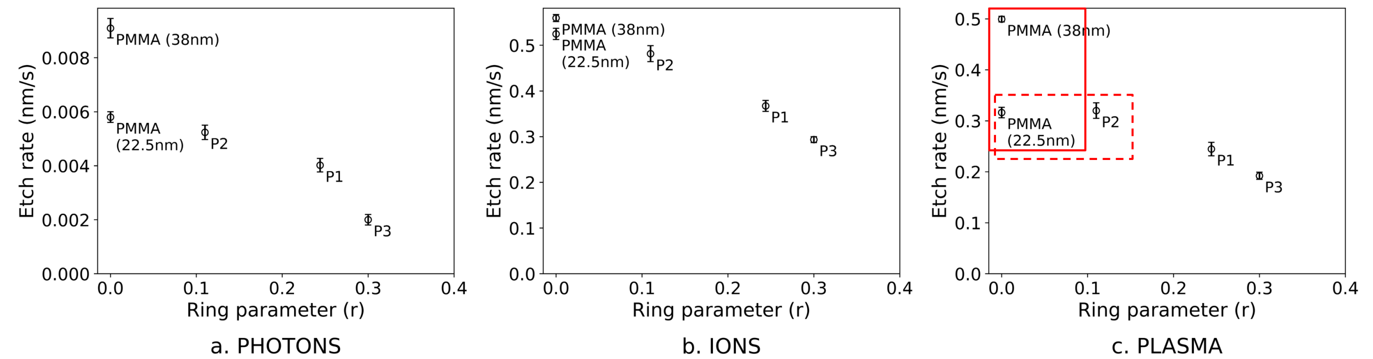

FIG. 9. Average etch rates of different resists compared with their ring parameter (r) under a. PHOTONS, b. IONS and c. PLASMA processing conditions. Solid box – thickness discrepancy of PMMA, Dashed box – discrepancy between P2 and thin PMMA.

[4]K. Du, J. Ying, L. Han, J. Xue, H. Xin, J. Zhang, and H. Li, "Accurate and efficient evaluation of the ionization potentials of extreme ultraviolet photoresists using density functionals and semi-empirical methods," Moore and More **1**, 3 (2024).

[5]D. F. Ogletree, "Chapter 2 - Molecular excitation and relaxation of extreme ultraviolet lithography photoresists," in *Frontiers of Nanoscience*, Materials and Processes for Next Generation Lithography, Vol. 11, edited by A. Robinson and R. Lawson (Elsevier, 2016) pp. 91–113.

[6]C. Mack, *Fundamental Principles of Optical Lithography: The Science of Microfabrication*, 1st ed. (Wiley, 2007).

[7]"Entering the High NA EUV Lithography era," https://www.imec-int.com/en/articles/entering-high-na-euv-lithography-era (2024).

[8]"High resolution lithography: Latest generation in EUV lithograph with 0.55 NA | SPIE Photomask Technology + EUV Lithography," https://spie.org/photomask-technology/presentation/High-resolution-lithography–Latest-generation-in-EUV-lithograph-with/13215-3 (2024).

[9]E. Van Setten, G. Bottiglieri, J. McNamara, J. Van Schoot, K. Troost, J. Zekry, T. Fliervoet, S. Hsu, J. Zimmermann, M. Roesch, B. Bilski, and P. Graeupner, "High NA EUV lithography: Next step in EUV imaging," in *Extreme Ultraviolet (EUV) Lithography X*, edited by K. A. Goldberg (SPIE, San Jose, United States, 2019) p. 5.

[10]A. Burov, A. Vaglio Pret, and R. Gronheid, "Depth of focus in high-NA EUV lithography: a simulation study," in *Photomask Technology 2022*, edited by B. S. Kasprowicz and T. Liang (SPIE, Monterey, United States, 2022) p. 46.

[11]H. Ito, "Chemical Amplification Resists for Microlithography," in *Microlithography · Molecular Imprinting*, Vol. 172 (Springer Berlin Heidelberg, Berlin, Heidelberg, 2005) pp. 37–245, collection-title: Advances in Polymer Science.

[12]E. Byun, S. Kim, S. Han, J. Choe, S. Kwon, J. H. Lee, and S. Choi, "Prediction of lithographic performance upon the adjustment of EUV photoresist components by advanced contrast curve analysis," in *Advances in Patterning Materials and Processes XLI*, edited by D. Guerrero and G. R. Amblard (SPIE, San Jose, United States, 2024) p. 58.

[13]S. Tarutani, W. Nihashi, S. Hirano, N. Yokokawa, and H. Takizawa, "Negative tone imaging process and materials for EUV lighography," (San Jose, California, USA, 2013) p. 868214.

[14]T. Fujimori, T. Tsuchihashi, and T. Itani, "Recent Progress of Negative-tone Imaging Process and Materials with EUV Exposure," Journal of Photopolymer Science and Technology **28**, 485–488 (2015).

[15]K. Ou, N. Tango, N. Fujimaki, K. Marumo, N. Hiura, S. Takahashi, and T. Fujimori, "A novel formulated developer for negative-tone imaging with EUV exposure to improve chemical stochastic," in *Advances in Patterning Materials and Processes XL*, edited by D. Guerrero and G. R. Amblard (SPIE, San Jose, United States, 2023) p. 11.

[16]R. Fallica, S. Chen, D. De Simone, and H. S. Suh, "Adhesion and collapse of extreme ultraviolet photoresists and the role of underlayers," Journal of Micro/Nanopatterning, Materials, and Metrology **21** (2022), 10.1117/1.JMM.21.3.034601.

[17]P. Vanelderen, N. Vandenbroeck, Y. Liang, V. Van Driessche, D. Guerrero, A. Chacko, D. De Simone, and G. Vandenberghe, "Underlayer optimization method for EUV lithography," in *Advances in Patterning Materials and Processes XXXVII*, edited by R. Gronheid and D. P. Sanders (SPIE, San Jose, United States, 2020) p. 39.

[18]Y. Liang, K. E. Brakensiek, J. Lowes, A. M. Chacko, R. Zhang, V. Van Driessche, X. Lang, J. Kasthuri, M. Luo, and D. J. Guerrero, "Realization of sub-15-nm half-pitch EUV lithography by the application of functional spin-on glass," in *Advances in Patterning Materials and Processes XXXIX*, edited by D. Guerrero and D. P. Sanders (SPIE, San Jose, United States, 2022) p. 19.

[19]M. Gupta, J. Antunes Afonso, P. Bézard, R. Vallat, R. Fallica, H. S. Suh, S. Halder, D. De Simone, Z. Liu, F. Ran, H. Fukuda, Y. Sun, D. De Roest,

ACCEPTED MANUSCRIPT
Journal of Vacuum Science & Technology A
This is the author's peer reviewed, accepted manuscript. However, the online version of record will be different from this version once it has been copyedited and typeset.
PLEASE CITE THIS ARTICLE AS DOI: 10.1116/6.0004265

and D. Piumi, "Scaled-down deposited underlayers for EUV lithography," in *Advances in Patterning Materials and Processes XL*, edited by D. Guerrero and G. R. Amblard (SPIE, San Jose, United States, 2023) p. 73.

[20] D. Popović, M. Mozetič, A. Vesel, G. Primc, and R. Zaplotnik, "Review on vacuum ultraviolet generation in low-pressure plasmas," Plasma Processes and Polymers **18**, 2100061 (2021), _eprint: https://onlinelibrary.wiley.com/doi/pdf/10.1002/ppap.202100061.

[21] S. Arvind, E. W. Larsen, P. Bezard, J. Petersen, and S. De Gendt, "Impact of vacuum ultraviolet photons on ultrathin polymethylmethacrylate during plasma etching," Journal of Vacuum Science & Technology A **42**, 033009 (2024).

[22] Z. el Otell, V. Šamara, A. Zotovich, T. Hansen, J.-F. de Marneffe, and M. R. Baklanov, "Vacuum ultra-violet emission of CF $_4$ and CF $_3$ I containing plasmas and Their effect on low-k materials," Journal of Physics D: Applied Physics **48**, 395202 (2015).

[23] J. B. Boffard, C. C. Lin, C. Culver, S. Wang, A. E. Wendt, S. Radovanov, and H. Persing, "Comparison of surface vacuum ultraviolet emissions with resonance level number densities. I. Argon plasmas," Journal of Vacuum Science & Technology A: Vacuum, Surfaces, and Films **32**, 021304 (2014).

[24] N. Vourdas, A. G. Boudouvis, and E. Gogolides, "Plasma etch rate measurements of thin PMMA films and correlation with the glass transition temperature," Journal of Physics: Conference Series **10**, 405–408 (2005).

[25] B. Li, S. Zhang, J. S. Andre, and Z. Chen, "Relaxation behavior of polymer thin films: Effects of free surface, buried interface, and geometrical confinement," Progress in Polymer Science **120**, 101431 (2021).

[26] M. Fouchier, E. Pargon, L. Azarnouche, K. Menguelti, O. Joubert, T. Cardolaccia, and Y. C. Bae, "Vacuum ultra violet absorption spectroscopy of 193 nm photoresists," Applied Physics A **105**, 399–405 (2011).

[27] G. S. Oehrlein, R. J. Phaneuf, and D. B. Graves, "Plasma-polymer interactions: A review of progress in understanding polymer resist mask durability during plasma etching for nanoscale fabrication," Journal of Vacuum Science & Technology B, Nanotechnology and Microelectronics: Materials, Processing, Measurement, and Phenomena **29**, 010801 (2011).

[28] J. Zekonyte, *Sputtering and Surface Modification of Thermoplastic Polymers with Low Energy Ion Beams*, Ph.D. thesis, Faculty of Engineering, Kiel University (2005).

[29] V. Kumar, B. Chaudhary, V. Sharma, and K. Verma, eds., *Radiation Effects in Polymeric Materials*, Springer Series on Polymer and Composite Materials (Springer International Publishing, Cham, 2019).

[30] C. Giori, T. Yamauchi, P. Llewellen, and J. Gilligan, "Fundamental investigation of ultraviolet radiation effects in polymeric film-forming materials," Tech. Rep. IITRI-C6295-10 (IIT RESEARCH INSTITUTE, Chicago, USA, 1974).

[31] H. Gokan, S. Esho, and Y. Ohnishi, "Dry Etch Resistance of Organic Materials," Journal of The Electrochemical Society **130**, 143–146 (1983).

[32] Q. Lin, "Properties of Photoresist Polymers," in *Physical Properties of Polymers Handbook*, edited by J. E. Mark (Springer, 2007) pp. 965–979.

[33] T. H. Fedynyshyn, R. R. Kunz, R. F. Sinta, R. B. Goodman, and S. P. Doran, "Polymer photochemistry at advanced optical wavelengths," Journal of Vacuum Science & Technology B: Microelectronics and Nanometer Structures Processing, Measurement, and Phenomena **18**, 3332–3339 (2000).

[34] E. Pargon, M. Martin, K. Menguelti, L. Azarnouche, J. Foucher, and O. Joubert, "Plasma impact on 193 nm photoresist linewidth roughness: Role of plasma vacuum ultraviolet light," Applied Physics Letters **94**, 103111 (2009).

[35] F. Weilnboeck, R. L. Bruce, S. Engelmann, G. S. Oehrlein, D. Nest, T.-Y. Chung, D. Graves, M. Li, D. Wang, C. Andes, and E. A. Hudson, "Photoresist modifications by plasma vacuum ultraviolet radiation: The role of polymer structure and plasma chemistry," Journal of Vacuum Science & Technology B, Nanotechnology and Microelectronics: Materials, Processing, Measurement, and Phenomena **28**, 993–1004 (2010).

[36] Y.-H. Ting, C.-C. Liu, S.-M. Park, H. Jiang, P. F. Nealey, and A. E. Wendt, "Surface Roughening of Polystyrene and Poly(methyl methacrylate) in Ar/O2 Plasma Etching," Polymers **2**, 649–663 (2010).

[37] A. R. Pal, R. L. Bruce, F. Weilnboeck, S. Engelmann, T. Lin, M.-S. Kuo, R. Phaneuf, and G. S. Oehrlein, "Real-time studies of surface roughness development and reticulation mechanism of advanced photoresist materials during plasma processing," Journal of Applied Physics **105**, 013311 (2009).

[38] D. Nest, D. B. Graves, S. Engelmann, R. L. Bruce, F. Weilnboeck, G. S. Oehrlein, C. Andes, and E. A. Hudson, "Synergistic effects of vacuum ultraviolet radiation, ion bombardment, and heating in 193nm photoresist roughening and degradation," Applied Physics Letters **92**, 153113 (2008).

[39] B. Jinnai, K. Koyama, K. Kato, A. Yasuda, H. Momose, and S. Samukawa, "Mechanism for low-etching resistance and surface roughness of ArF photoresist during plasma irradiation," Journal of Applied Physics **105**, 053309 (2009).

[40] M. P. Seah, "Universal Equation for Argon Gas Cluster Sputtering Yields," The Journal of Physical Chemistry C **117**, 12622–12632 (2013).

[41] D. Metzler, F. Weilnboeck, S. C. Hernández, S. G. Walton, R. L. Bruce, S. Engelmann, L. Salamanca-Riba, and G. S. Oehrlein, "Formation of nanometer-thick delaminated amorphous carbon layer by two-step plasma processing of methacrylate-based polymer," **33**, 051601.

[42] A. Pranda, S. A. Gutierrez Razo, Z. Tomova, J. T. Fourkas, and G. S. Oehrlein, "Role of the dense amorphous carbon layer in photoresist etching," **36**, 021304.

[43] G. K. Choudhary, J. J. Végh, and D. B. Graves, "Molecular dynamics simulations of oxygen-containing polymer sputtering and the Ohnishi parameter," **42**, 242001.

[44] M. J. Bowden, E. A. Chandross, and I. P. Kaminow, "Mechanism of the Photoinduced Refractive Index Increase in Polymethyl Methacrylate," Applied Optics **13**, 112 (1974).

[45] W. J. Tomlinson, I. P. Kaminow, E. A. Chandross, R. L. Fork, and W. T. Silfvast, "Photoinduced refractive index increase in Poly(Methylmethacrylate) and its applications," Applied Physics Letters **16**, 486–489 (1970).

[46] C. Wochnowski, S. Metev, and G. Sepold, "Uv–laser-assisted modification of the optical properties of polymethylmethacrylate," Applied Surface Science **154-155**, 706–711 (2000).

[47] J.-g. Liu and M. Ueda, "High refractive index polymers: fundamental research and practical applications," Journal of Materials Chemistry **19**, 8907 (2009).

[48] D. J. Economou, "Tailored ion energy distributions on plasma electrodes," Journal of Vacuum Science & Technology A: Vacuum, Surfaces, and Films **31**, 050823 (2013).

[49] J. F. Ziegler, J. P. Biersack, and M. D. Ziegler, *SRIM, the Stopping and Range of Ions in Matter* (SRIM Company, 2008) google-Books-ID: JSN63qxPG5MC.

[50] D. Fink, ed., *Fundamentals of Ion-Irradiated Polymers*, Springer Series in Materials Science, Vol. 63 (Springer Berlin Heidelberg, Berlin, Heidelberg, 2004) dOI: 10.1007/978-3-662-07326-1.

[51] K. J. Orvek and C. Huffman, "Carbonized layer formation in ion implanted photoresist masks," Nuclear Instruments and Methods in Physics Research Section B: Beam Interactions with Materials and Atoms **7-8**, 501–506 (1985).

[52] P. Gröning, O. Küttel, M. Collaud-Coen, G. Dietler, and L. Schlapbach, "Interaction of low-energy ions (< 10 eV) with polymethylmethacrylate during plasma treatment," Applied Surface Science **89**, 83–91 (1995).

[53] B. C. Smith, *Infrared Spectral Interpretation: A Systematic Approach* (CRC Press, 1999).

[54] B. Jinnai, T. Uesugi, K. Koyama, K. Kato, A. Yasuda, S. Maeda, H. Momose, and S. Samukawa, "Decisive factors affecting plasma resistance and roughness formation in ArF photoresist," Journal of Physics D: Applied Physics **43**, 395204 (2010).

[55] F. Weilnboeck, N. Kumar, G. S. Oehrlein, T.-Y. Chung, D. Graves, M. Li, E. A. Hudson, and E. C. Benck, "Real-time measurements of plasma photoresist modifications: The role of plasma vacuum ultraviolet radiation and ions," Journal of Vacuum Science & Technology B, Nanotechnology and Microelectronics: Materials, Processing, Measurement, and Phenomena **30**, 031807 (2012).

[56] T. Uesugi, T. Okada, A. Wada, K. Kato, A. Yasuda, S. Maeda, and S. Samukawa, "The effects of polymer side-chain structure on roughness formation of ArF photoresist in plasma etching processes," Journal of Physics D: Applied Physics **45**, 075203 (2012).

[57] R. R. Kunz, S. C. Palmateer, A. R. Forte, R. D. Allen, G. M. Wallraff, R. A. Di Pietro, and D. C. Hofer, "Limits to etch resistance for 193-nm single-layer resists," (Santa Clara, CA, 1996) p. 365.

[58] T. I. Wallow, P. J. Brock, R. A. D. Pietro, R. D. Allen, J. Opitz, R. Sooriyakumaran, D. C. Hofer, A. M. Mewherter, Y. Cui, W. Yan, G. Worth, W. M. Moreau, J. Meute, J. D. Byers, G. K. Rich, M. McCallum, S. Jayaraman, R. Vicari, J. Cagle, S. Sun, and K. A. Hullihen, "Development of an incremental structural parameter model for predicting reactive

Journal of Vacuum Science & Technology A
ACCEPTED MANUSCRIPT
This is the author's peer reviewed, accepted manuscript. However, the online version of record will be different from this version once it has been copyedited and typeset.
PLEASE CITE THIS ARTICLE AS DOI: 10.1116/6.0004265

ion etch rates of 193-nm photoresist polymer platforms," in *Advances in Resist Technology and Processing XVI*, Vol. 3678 (SPIE, 1999) pp. 26–35.

[59] S. Kishimura, M. Endo, and M. Sasago, "New 157-nm resist platform based on etching model for fluoropolymers," in *Advances in Resist Technology and Processing XIX*, Vol. 4690 (SPIE, 2002) pp. 200–211.

[60] Y. Kawaguchi, J. Irisawa, S.-i. Kodama, S. Okada, Y. Takebe, I. Kaneko, O. Yokokoji, S. Ishikawa, S. Irie, T. Hagiwara, and T. Itani, "Dry-etching resistance of fluoropolymers for 157-nm single-layer resists," (Santa Clara, CA, 2003) p. 43.

[61] K. S. Patel, V. Pham, W. Li, M. Khojasteh, and P. R. Varanasi, "Reactive ion etching of fluorine containing photoresist," (San Jose, CA, 2006) p. 61530Q.

[62] D. Perret, C. E. Andes, K.-S. Cheon, M. Sobhian, C. R. Szmanda, G. G. Barclay, and P. Trefonas, "Etch resistance: comparison and development of etch rate models," (San Jose, CA, 2007) p. 651912.

[63] R. Huang and M. Weigand, "Plasma etch properties of organic BARCs," (San Jose, California, USA, 2008) p. 69232G.

[64] A. Bard, K. K. Berggren, J. L. Wilbur, J. D. Gillaspy, S. L. Rolston, J. J. McClelland, W. D. Phillips, M. Prentiss, and G. M. Whitesides, "Self-assembled monolayers exposed by metastable argon and metastable helium for neutral atom lithography and atomic beam imaging," Journal of Vacuum Science & Technology B: Microelectronics and Nanometer Structures Processing, Measurement, and Phenomena **15**, 1805–1810 (1997).